Formation mechanism of β”-Mg5Si6 and its PFZ in an Al-Mg-Si-Mn alloy: experiment and first-principles calculations

Xiaoming Qian
Yanshan University
Yong Li
Northeastern University
Zhaodong Wang (zhaodongwang@263.net)
Northeastern University

Research Article

Keywords: precipitation free zone (PFZ), β”-Mg5Si6, vacancy, first-principles calculations

Posted Date: November 9th, 2021

DOI: https://doi.org/10.21203/rs.3.rs-1036479/v1

Formation mechanism of β''-Mg_5Si_6 and its PFZ in an Al-Mg-Si-Mn alloy: experiment and first-principles calculations

Xiaoming Qian [a], Yong Li [b, c, *], Zhaodong Wang [b, **]

[a] National Engineering Research Center for Equipment and Technology of Cold Strip Rolling, Yanshan University, Qinhuangdao 066004, China

[b] State Key Laboratory of Rolling and Automation, Northeastern University, Shenyang 110819, China

[c] Guangxi Advanced Aluminum Processing Innovation Center Co. LTD, Nanning 530007, China

[*]Correspondence author: liyong.neu@163.com, zhaodongwang@263.net

Abstract

Formation mechanism of β''-Mg_5Si_6 and its PFZ in an Al-Mg-Si-Mn alloy was studied by the means of experiment and first-principles calculations. Results show that at 270°C during the 100 °C/h heating period, β''-Mg_5Si_6 precipitated inside the dendrites, whereas precipitation free zones (PFZs) of β''-Mg_5Si_6 presented near the dendrite arm regions. The formation of the β''-Mg_5Si_6 and its PFZ were related to the concentration of vacancy. Low-concertation zones of vacancy formed near the eutectics during the solidification due to the constitutional supercooling, no β''-Mg_5Si_6 precipitated in the low-concertation zones of vacancy due to the vacancy-dependence of β''-Mg_5Si_6, the Si vacancy-containing β''-Mg_5Si_6 was extremely unstable and Si vacancies prefer to stay away from distribution.

Key words: precipitation free zone (PFZ), β''-Mg_5Si_6, vacancy, first-principles calculations

1. Introduction

Dispersoids-strengthened alloys refer to the resistance to motion of dislocations is increased by introducing finely divided hard particles of second phase in the metal matrix. In our previous study [1], 6082 alloys strengthened via α-Al(Fe, Mn)Si dispersoids were developed by adding Mn in 6082 alloys and by performing an ultra-low-temperature homogenization during which a number of α-Al(Fe, Mn)Si dispersoids precipitated, these dispersoids exerted a significant increase in flow stresses and hot deformation activation energy of the alloys. In our further investigation on the α-Al(Fe, Mn)Si dispersoids [2], uniformly distribution of the dispersoids was found, precipitation-free zones (PFZs) emerged near the interdendritic regions. These PFZs of dispersoid brought a consequence that local recrystallization occurred in the PFZs during the subsequent annealing due to the absence of dispersoids and the weakened recrystallization resistance.

Generally, PFZs are not preferable in the structure material, they were thought to be ‘‘weak zones’’ in alloys since they are often softer than other regions in the matrix [3, 4]. It is reported that the mechanical behavior, fracture resistance, and stress corrosion cracking resistance of alloys had a close relationship with PFZ features [5-7]. Two mechanisms were put forward to account for PFZ formation: vacancy depletion and solute depletion. The vacancy depletion mechanism takes the effects of vacancy sinks during quenching into account, which results in retarded precipitation around grain boundaries compared with that in the inner grain [8]. Under the solute depletion mechanism, the suppressed precipitation around grain boundaries is attributed to the decreased supersaturation of solute atoms, which is frequently induced in conjunction with the formation of more stable, coarsened grain boundary precipitates [9].

So far, the formation mechanism of PFZ about α-Al(Fe, Mn)Si dispersoids was not able to found in the literatures, however, the formation of α-Al(Fe, Mn)Si dispersoid itself has been studied by researchers. Li [10] suggested that during the heating stage of homogenization, Mg- and Si- bearing β’’ phase precipitated along the <100>Al direction at 275℃ and then dissolved when the temperature reached 375℃. The dissolution of β’’ phase created a lath-like “Si”-rich region at the former position. These lath-like “Si”-rich region thus provided favorable sites for the nucleation of α-Al(Fe, Mn)Si and resulted the α-Al(Fe, Mn)Si dispersoids formed and grow along the <001>Al direction in the previous Si-rich sites. Hu [11] suggested that the needl-like β’ phase is strongly affected by the heating rate of the homogenization, a slower heating rate of homogenization in Al-Mg-Si-Mn alloy is favorable than the fast-heating rate in aspect of generating fine and dense of β’ phase. Lars Lodgaard et. al [12] provided some evidence that a “u-phase” was formed during homogenization, after continuous heating to 400°C during homogenization with a heating rate of 3K/min, a series of intermediate “u-phase” was formed, the “u-phase” has a hexagonal unit cell and was located lined up in the [100] directions of in the Al lattice since they were nucleated on the pre-existed β’ needles. The meta-stable Mg-and Si-bearing particle played significant roles on the α-Al(Fe, Mn)Si dispersoids in dispersoid-strengthened Al-Mg-Si-Mn alloys.

Since the development of the α-Al(Fe, Mn)Si dispersoid-strengthened alloys several years ago, investigation focusing on promoting the dispersoid number density and improving the mechanical properties have been carried out [10, 13,14], however, the PFZ of the dispersoids had not been drawn enough attention. To date, no detailed study about the formation of its PFZ has been carried out by the means of first-principles calculations. Actually, the PFZ was one of the key factors relating to the mechanical behavior, fracture resistance, and stress corrosion cracking resistance of alloys [15, 16]. Therefore, the formation mechanism of the β’’-Mg_5Si_6 phase and its PFZ should be better understood.

In this study, a systematic investigation on the microstructure evolution refers to the Mg- and Si-containing particles and its PFZ during homogenization was performed. First-principles calculation involving the β’’-Mg_5Si_6 was performed. The focus was particularly placed on the relationship between vacancy, β’’-Mg_5Si_6 and its PFZ.

2. Experimental and calculation methods

Experiments were carried out on an Al-0.8Mg-0.75Si-0.75Fe-1Mn (in wt.%) alloy. A rectangular plate measuring 200 mm ×100 mm ×7 mm was cast using a sand mold, the cooling rate of the solidification was tested to be 1.4 °C/s. An ultra-low-temperature homogenization at 430 °C for 6 h was conducted to promote the precipitation of dispersoids. A heating rate of 100 °C/h was set to further enhance dispersoid precipitation [1, 2, 11]. Quenching at 250, 270 and 300°C during heating stage was performed to verify the microstructural evolution. An optical microscope (Leica DMI5000M), a scanning electron microscope (Shimadzu, SSX-550) equipped with an energy-dispersive X-ray spectrometer and a transmission electron microscope (JEM-2100) were used for the microstructural observations. To reveal the precipitation particles, the surfaces of some polished specimens were etched with 0.5% HF solution for 30 s. Emission electron probe microanalysis (EPMA) was used to measure the alloying element distributions.

The first-principles calculations performed in the present work were based on the density functional theory (DFT) by the use of the Vienna ab initio Simulation Package (VASP) [17]. The interaction between ions and electrons was described by the projector-augmented wave method [18], and the exchange-correlation potential was treated by the Perdew–Burke–Ernzerhof (PBE) implementation of generalized gradient approximation (GGA) [19]. The $3s^2$ and $3s^23p^2$ were treated as valence states for Mg and Si. The energy of the cut-off was 319 eV. A Monkhorst–Pack grid was employed to sample the Brillouin zone [20], and the 4×16×10 k-point grids was used to calculate the β''- Mg_5Si_6 and its vacancy structure. During the structural optimization, the criteria for the total energies and the forces on individual atoms were set to 1 meV and 0.02 eV/Å, respectively.

3. Results and discussions

3.1 Microstructure evolution during homogenization

Homogenization treatment was conduct with a heating rate of 100 °C/h. Fig.1 shows the microstructural evolution. Fig. 1a shows the microstructure of the sample when the temperature reached 250°C during heating, the microstructure is consistent with the Al matrix and eutectics distributed along the dendrite boundaries. With the increasing of temperature to 270°C (Fig. 1b), large number of fine precipitates was observed inside the dendrites, whereas precipitation free zones (PFZs) presented near the dendrite arm regions. The inset TEM image shows the morphology of the precipitation, the particles are lath-like and are approximately 25 nm in width and about 300 to 500 nm in length which located along with the <100>Al directions, the black dots represent the cross sections. These precipitates were identified to be β'' -Mg_5Si_6 phase according to the corresponding selected area diffraction pattern (SADP, Fig inset in Fig. 1b, as indicated by the red circles) [10, 21]. When the temperature reached 300°C during the heating stage of homogenization (Fig. 1c), the OM microstructure shows

limit variation with that of 270°C condition, however, in the TEM image (as inset of Fig. 1c), partially dissolution of the β'' phase was observed. It is noticeable that some dot-like particles emerged on the position of the pre-existed β''-Mg_5Si_6. After 6h hold at 430°C (Fig. 1d), PFZ could be still observed in the OM image. In the inset TEM image, it is found that the particles appeared in various shapes, mostly short-plates and rods, It is distinguishable that these particles mainly located along with the <001>Al direction. The particles were confirmed to α-Al(Fe, Mn)Si dispersoids according to previous studies [1, 2].

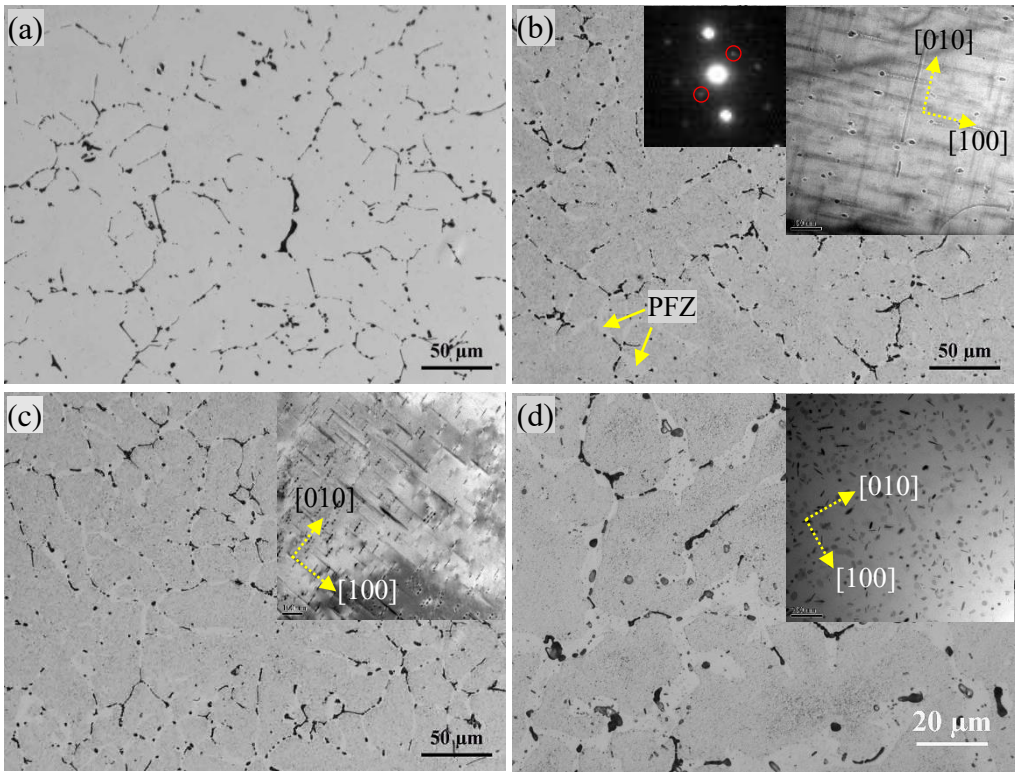

Fig. 1 OM image of the sample when the temperature reached (a) 250°C, (b) 270°C, (c) 300°C during heating; (d) after 6h hold at 430°C. TEM image were inset, the selected area diffraction pattern was from the particles in the TEM image of (b), β'' phase was indicated by the red circles.

3.2 β''- Mg_5Si_6 and its PFZ

During the heating stage of homogenization, the supersaturated solid solution of Mg and Si created during casting decompose and β''-Mg_5Si_6 precipitated (Fig.1). Inhomogeneous distributions of β''-Mg_5Si_6 was a result of the performance differences between the region inside the dendrites and the region near dendrite arms and intermetallics. In general, the formation of PFZ could be attributed to lack of particle former elements and/or heterogeneous nucleation sites [8, 9]. Emission electron probe analysis (EPMA) was carried out to check the alloying element concentrations of the as-cast alloy. The chosen positions for the test are shown in Fig. 2. Four points were set as the test positions: points 1 and 4 were set inside the dendrites, while points 2 and 3

were located near the intermetallics. The results of EPMA are shown in Table 1. As indicated, uneven distribution of alloying elements of Mg, Si, Fe and Mn was found, all the alloying element exhibited higher concentrations at the regions near dendrite arms than the positions inside the dendrites. For example, concentrations of Mg and Si at the dendrites arm region (position 2 and 3) were 0.522-0.594, while it decreased to 0.215-0.217 at the region inside dendrites (position 4 and 1). This result, the element of Mg and Si was not deficient at the position of β'' PFZ formed, but even in a higher concentration, excluded the possibility that the β'' PFZ was attributed to the lack of alloying elements.

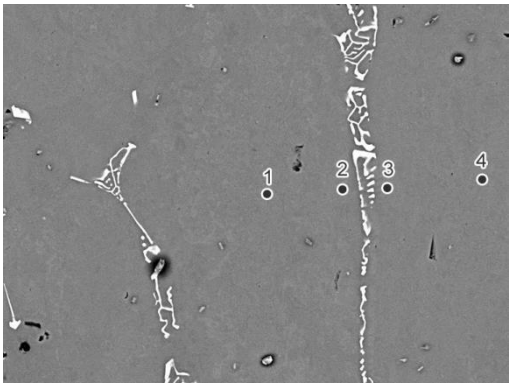

Fig. 2 EPMA positions of the as-cast sample.

Table. 1 Alloying element content (wt.%) at different positions in Fig. 2

Position	1	2	3	4
Mg	0.217	0.522	0.594	0.215
Si	0.268	0.572	0.578	0.273
Fe	0.010	0.056	0.068	0.012
Mn	0.481	0.656	0.587	0.476

The higher concentration of alloying elements at the dendrites arm regions than that inside the dendrites could be explained by the classic solidification theory. As illustrated in Fig. 3, during the eutectic reaction of solidification, the alloying elements are released to the liquid from the interface of the solid and liquid. Along with the ongoing solidification, more alloying elements were accumulated at grooves where the boundaries of dendrites arms were formed. With the finishing of solidification, the high concentration of solutes was squeezed into the boundaries dendrites arms, thus formed the high concentration region of alloying elements at the dendrite are regions [22].

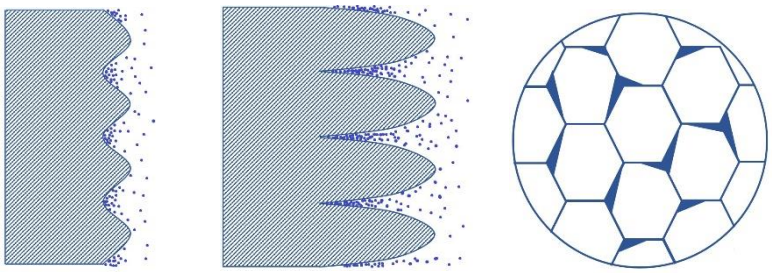

Fig. 3 Schematic of the process of solidification

The nonuniformly distribution of the solutions in the Al dendrites was accompanied with the vary of solidification and the concentration of vacancy. Fig. 4 shows a phase diagraph illustrating a typical eutectic solidification. The primary Al crystal formed at the temperature of liquid line. Along with the solidification, as the solutes were pushed to the liquid phase, the solution concentration increased and the Ts reduced accordingly, which is referred as "constitutional supercooling" [23, 24].

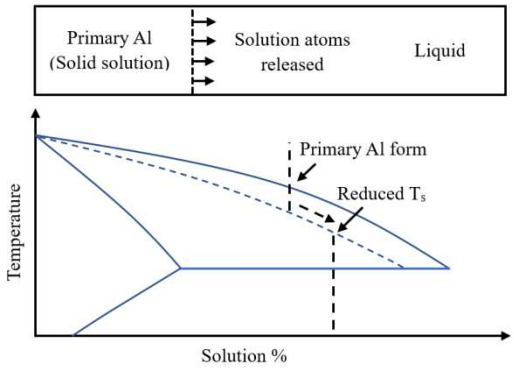

Fig. 4 Phase diagraph illustrating typical eutectic solidification

Based on the relationship between the solidification temperature and vacancy, the concentration of vacancy declined with the decreasing solidification temperatures, it was inferred that the concentrations of vacancy at the region near eutectic were lower than those at the region inside the dendrites, that was, the vacancy concentration positions 2 and 3 in Fig. 2 were lower than those of positions 1 and 4.

The demonstration above suggested that the at the region near dendrite arms where PFZ of β'' and α-Al(Fe, Mn)Si dispersoid emerged, the alloying elements was

accumulated during the eutectic solidification, which led a consequence that the overall lowered solidification temperature and concentration of vacancy at the region near dendrite arms than that inside the dendrites.

3.3 First-principles calculations: vacancy and β''-Mg_5Si_6

In order to verify the relationship between the vacancy and β'', the first-principles calculations were carried out. Here we use the defect formation energy to express the stability of the structure. Defect formation can be calculated by the following equation [25]:

$$E_f = E_{def} - E_{id} + n_{Mg}\mu_{Mg} + n_{Si}\mu_{Si}$$

where E_f is the defect formation energy; E_{def} and E_{id} are the total energies of the defective and ideal unit cell, respectively; n_{Mg} and n_{Si} are the number of Mg and Si atoms which is transferred to or from a chemical reservoir; μ_{Mg} and μ_{Si} are the corresponding chemical potential of the pure element.

The optimized lattice constants of the β''-Mg_5Si_6 structure are a=15.01, b=4.07, c=6.87, and β=107.3°. This is very close to the experimental values (a=15.16, b=4.05, c=6.74, and β=105.3°) [26, 27]. The relative errors for a, b, and c are 0.98%, 0.49% and 1.89% respectively, and that of the monoclinic angle β is 1.86%. The above results prove the accuracy of the calculations.

Fig. 5 shows the formation energies of the β''-Mg_5Si_6 and its vacancy structures. As can be seen from the figure, β''-Mg_5Si_6 structure has the lowest formation energy, indicating that the structure is the most stable at this point. With the formation energy gradually increasing as the vacancy concentration increases, leading to a substable state for the vacancy-containing β''-Mg_5Si_6 structure. The Si vacancy-containing β''-Mg_5Si_6 structure is the most unstable, implying that the Si vacancy-containing precipitates are extremely unstable and thus it can be preferentially precipitated, which is consistent with the experimental observations (Fig. 1).

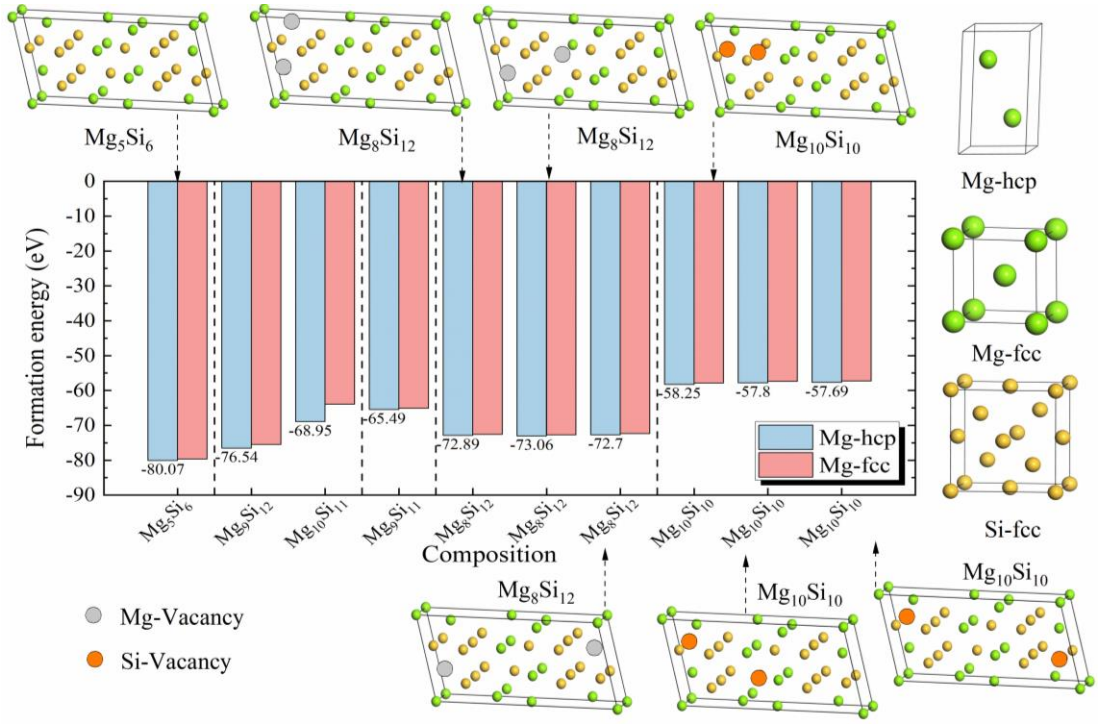

Fig. 5 Illustrations of the Mg_5Si_6, the Mg-vacancy, and Si-vacancy. Formation energies of Mg_5Si_6 structure and containing-vacancy in Mg_5Si_6 structure.

Subsequently, the variation of the formation energy with the degree of aggregation of Mg or Si atoms was calculated. The degree of atomic aggregation is divided into three main cases: aggregated, uniform, and distant distributions. The results show that both Mg vacancies and Si vacancies are most unstable when distant distributed. These are extremely easy to observe experimentally (Fig. 1).

4. Conclusions

An Al-Mg-Si-Mn alloy was prepared and an ultra-low-temperature homogenization at 430 °C for 6 h was conducted. Formation mechanism of β''-Mg_5Si_6 and its PFZ in an Al-Mg-Si-Mn alloy was studied by means of experiment and first-principles calculations. The following conclusions were drawn:

(1) At 270°C during the 100 °C/h heating, β''-Mg_5Si_6 precipitated inside the dendrites, whereas precipitation free zones (PFZs) of β''-Mg_5Si_6 presented near the dendrite arm regions. After homogenization at 430°C for 6h, α-Al(Fe, Mn)Si dispersoids formed inside the dendrites while the PFZs of α-Al(Fe, Mn)Si were located near the dendrite arm regions.

(2) The element of Mg and Si at the regions near the dendrite arms were higher than the regions inside dendrites, which excluded the possibility that the β''-Mg_5Si_6 PFZ was attributed to the lack of alloying elements.

(3) Low-concertation zones of vacancy formed near the eutectics during the solidification due to the constitutional supercooling, no β''-Mg_5Si_6 precipitated in the low concertation zones of vacancy owing to the vacancy acted as the nucleation sites for the precipitation of β''-Mg_5Si_6.

(4) The results of first-principles calculations show that the Si vacancy-containing precipitates are extremely unstable and Si vacancies prefer to stay away from distribution, which further confirmed the vacancy-dependence of β''-Mg_5Si_6 precipitation and explained the formation of PFZs of β''-Mg_5Si_6 and α-Al(Fe, Mn)Si dispersoids.

Acknowledgements

The authors gratefully acknowledge the support of the National Natural Science Foundation of China (Grant No. 51790485), the Fundamental Research Funds for the Central Universities (No. N2007008), Nanning science and technology major special projects (No. 20201041) and the Key research and development project of Shandong province (No. 2019JZZY010401).

References

[1] X. Qian, N. Parson, X.G. Chen, Effects of Mn addition and related Mn-containing dispersoids on the hot deformation behavior of 6082 aluminum alloys, Materials Science and Engineering: A 764 (2019) 138253.

[2] X. Qian, N. Parson, X.G. Chen, Effects of Mn content on recrystallization resistance of AA6082 aluminum alloys during post-deformation annealing, Journal of Materials Science & Technology 52 (2020) 189–197.

[3] J. Corral, E.A. Trillo, Y. Li, L.E. Murr, Corrosion of friction-stir welded aluminum alloys 2024 and 2195, Journal of Mater. Sci. Let., 19 (2000) 2117–2122.

[4] I.N. Fridlyand, A.M. Drits, A.A. Yeliseyev, Lightweight and high-temperature alloys and the processing of them, Nauka, Moscow (1986) 126-130.

[5] Y.W. Riddle, T.h. Sanders, A study of coarsening, recrystallization, and morphology of microstructure in Al-Sc-(Zr)-(Mg) alloys, Metal. Mater. Trans. A, 35 (2004) 341-350.

[6] R.R. Sawtell, C.L. Jensen, Mechanical properties and microstructures of Al-Mg-Sc alloys, Metal. Trans. A, 21 (1990) 421-430.

[7] K.H. Chen, H.C. Fang, Z. Zhang, X. Chen, G. Liu, Effect of of Yb, Cr and Zr additions on recrystallization and corrosion resistance of Al–Zn–Mg–Cu alloys, Mater. Sci. Eng. A, 497 (2008) 426–431.

[8] A. Zindal, J. Jain, R. Prasad, S.S. Singh, R. Sarvesha, P. Cizek, M.R. Barnett, Effect of heat treatment variables on the formation of precipitate free zones (PFZs) in Mg-8Al-0.5Zn alloy, Materials Characterization 136 (2018) 175–182.

[9] Y.J. Li, L. Arnberg, Quantitative study on the precipitation behavior of dispersoids in DC-cast AA3003 alloy during heating and homogenization, Acta Materialia 51 (2003) 3415–3428.

[10] Z. Li, Z. Zhang, X. G. Chen, Effect of Metastable Mg2Si and Dislocations on α-Al(MnFe)Si Dispersoid Formation in Al-Mn-Mg 3xxx Alloys, Metallurgical and Materials Transactions A 49A (2018) 5799.

[11] R. Hu, T. Ogura, et al. Dispersoid Formation and Recrystallization Behavior in an

Al-Mg-Si-Mn Alloy, Journal of Materials Science & Technology 26(3) (2010) 237-243.
[12] L. Lodgaard, N. Ryum, Precipitation of dispersoids containing Mn and/or Cr in Al–Mg–Si alloys, Materials Science and Engineering: A 283 (2000) 144–152.
[13] K. Liu, X.Grant Chen, Development of Al–Mn–Mg 3004 alloy for applications at elevated temperature via dispersoid strengthening,Transactions of Nonferrous Metals Society of China 26 (2016) 2793−2799.
[14] K. Liu, Hezhaoye Ma, X. Grant Chen, Enhanced elevated-temperature properties via Mo addition in Al-Mn-Mg 3004 alloy, Journal of Alloys and Compounds 694 (2017) 354-365.
[15] K.H. Chen, H.C. Fang, Z. Zhang, X. Chen, G. Liu, Effect of of Yb, Cr and Zr additions on recrystallization and corrosion resistance of Al–Zn–Mg–Cu alloys, Mater. Sci. Eng. A, 497 (2008) 426–431.
[16] M. B. Kannan, V.S. Raja, Enhancing stress corrosion cracking resistance in Al–Zn-Mg-Cu-Zr alloy through inhibiting recrystallization, Eng. Fracture Mech. 77 (2010) 249–256.
[17] G. Kresse, D. Joubert, From ultrasoft pseudopotentials to the projector augmented-wave method, Phys. Rev. B. 59 (1999) 1758-1775.
[18] P.E. Blochl, Projector augmented-wave method, Phys. Rev. B. Condens. Matter. 50 (1994) 17953-17979.
[19] J. P. Perdew, K. Burke, M. Ernzerhof, Generalized Gradient Approximation Made Simple, Phys. Rev. L. 77 (1996) 3865-3868.
[20] H.J. Monkhorst, J.D. Pack, Special points for Brillouin-zone integrations, Phys. Rev. B. 13 (1976) 5188-5192.
[21] Y. Wang, Z.-K. Liu, L.-Q. Chen, C. Wolverton, First-principles calculations of β'' -Mg5Si6/α-Al interfaces, Acta Materialia 55 (2007) 5934–5947
[22] S.J. Li, G.M. Xu, Y. Li, Z.D. Wang, et al., Effects of different external fields on the microstructure and mechanical properties of novel Al-Cu-Li alloy during twin-roll casting, Materials Science & Engineering A 757 (2019) 14–22
[23] S. Yuan, X. Yu, D. Hu et al., Defect control based on constitutional supercooling effect in cast multicrystalline silicon: Boron-indium co-doping, Solar Energy Materials and Solar Cells 203 (2019) 110189
[24] M. Qian, P. Cao, M.A. Easton et al., An analytical model for constitutional supercooling-driven grain formation and grain size prediction, Acta Materialia 58 (2010) 3262–3270
[25] J. Bai, J. M. Raulot, Y. D. Zhang, C. Esling, X. Zhao, and L. Zuo, Defect formation energy and magnetic structure of shape memory alloys Ni–X–Ga (X=Mn, Fe, Co) by first principle calculation, J. Appl. Phys. 108 (2010) 064904
[26] P. M. Derlet, S . J. ANDERSEN, C. D. MARIOARA and A. FRØSETH, J. Phys.: Cond. Matter. 14 (2002) 4011. 7
[27] S . J. ANDERSEN, H. W. ZANDBERGEN, J. JANSEN, C. T R Æ H O LT, U. TUNDAL and O. REISO, Acta Mater. 46 (1998) 328